Bulletin of the Seismological Society of America, Vol. 99, No. 1, pp. 87–94, February 2009, doi: 10.1785/0120080192

The M_w 7.7 Tocopilla Earthquake of 14 November 2007 at the Southern Edge of the Northern Chile Seismic Gap: Rupture in the Deep Part of the Coupled Plate Interface

by Bertrand Delouis, Mario Pardo, Denis Legrand,* and Tony Monfret

Abstract The slip distribution of the M_w 7.7 Tocopilla earthquake was obtained from the joint inversion of teleseismic and strong-motion data. Rupture occurred as underthrusting at the base of the seismically coupled plate interface, mainly between 35 and 50 km depth. From the hypocenter, located below the coast 25 km south of the town of Tocopilla, the rupture propagated 50 km northward and 100 km southward. Overall, the slip distribution was dominated by two slip patches, one near the hypocenter and the other 70 km to the south where slip reached its maximum value (3 m). An additional branch of moderate slip propagated at shallower depth toward the west near the northern tip of the Mejillones peninsula. Rupture velocity remained close to 2.8 km/sec, with a total rupture duration of 45 sec. The first 2 weeks of aftershocks located with a local seismic network display a strong correlation with the slip distribution. The 2007 rupture ended below the Mejillones peninsula, where the 1995 Antofagasta rupture also ended (Ruegg *et al.*, 1996; Delouis *et al.*, 1997; Pritchard *et al.*, 2006). This corroborates the role of barrier played by this structure. The downdip end of the seismically coupled zone at 50 km depth, evidenced by previous studies for the 1995 event, is also confirmed. The 2007 Tocopilla earthquake contributed only moderately to the rupturing of the great northern Chile seismic gap, which still has the capacity for generating a much larger underthrusting event.

Introduction

The large M_w 7.7 Tocopilla earthquake of 14 November 2007 (15:41 UTC) occurred in the Antofagasta region of northern Chile. The epicenter obtained in this study is located 25 km south of the small town of Tocopilla and 150 km north-northeast of the city of Antofagasta (Fig. 1). The Global Centroid Moment Tensor (GCMT) catalog solution for the mainshock (see the Data and Resources section), with a centroid depth of 38 km and a focal mechanism showing a low-angle nodal plane with reverse motion, suggests that this event should be categorized as a subduction underthrusting earthquake occurring at the interface between the subducting Nazca plate and the overriding South American plate. According to background seismicity and focal mechanisms distribution, the plate interface in this area was recognized to be seismically coupled between 20 and 50 km depth (Comte and Suárez, 1995; Delouis *et al.*, 1996), and the rupture of large underthrusting earthquakes can be expected to take place in this depth interval. In northern Chile, the shallow part of the subduction interface remains essentially unruptured since the M 9 earthquake of 1877, and the region is identified as a major seismic gap (Comte and Pardo, 1991). Before the 2007 earthquake, the gap could be drawn approximately from 23° S (Mejillones/Antofagasta) to 18° S (Ilo, southern part of the 2001 Arequipa earthquake, G1 in Fig. 1). The Tocopilla earthquake occurred in the southern part of the gap. Despite its large magnitude it generated only a small tsunami wave (height <30 cm; U.S. Geological Survey [USGS], 2007a).

Fast source inversions of the 14 November 2007 earthquake based on teleseismic data (USGS, 2007b; Vallée, 2007) indicate that rupture propagation occurred mainly toward the south, with two or three individualized slip patches. In this study, we perform a joint inversion of teleseismic and strong-motion data. Six digital accelerometers, among which two are situated above the rupture plane (TOCO, MEJI in Fig. 1a), provide a reinforced control on the location of the mainshock hypocenter (rupture initiation) and on the absolute location of slip. We show that the joint inversion of the two datasets improves the resolution of the slip distribution. The first 2 weeks of the aftershock sequence are analyzed using local

*Present address: Universidad Nacional Autónoma de México (UNAM), Instituto de Geofisica, Departamento de Vulcanologia, Ciudad Universitaria, Del. Coyoacan México D.F., C.P. 04510, denis@geofisica.unam.mx.

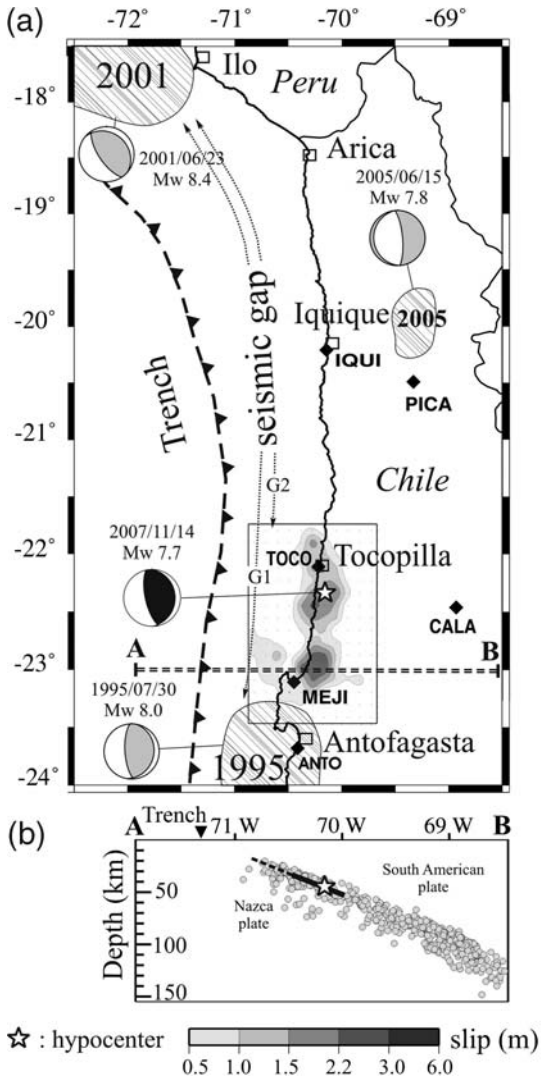

Figure 1. Situation map of northern Chile–southern Peru. The terminations of the 1995 Antofagasta (M_w 8.0) and 2001 Arequipa (M_w 8.4) interplate earthquake ruptures are indicated, as well as the 2005 Tarapaca (M_w 7.8) intermediate-depth earthquakes rupture zone (hatched surfaces labeled 1995, 2001, and 2005, respectively, Ruegg *et al.*, 1996; Delouis *et al.*, 1997; Pritchard *et al.*, 2006; Bilek and Ruff, 2002; Delouis and Legrand, 2007). The gray contoured areas in the rectangular frame correspond to the surface projection of the slip model obtained in this study for the 2007 Tocopilla earthquake. The double dashed line AB indicates the cross-section line of (b). Also displayed, the focal mechanism here determined for the Tocopilla mainshock, in black, and the focal mechanisms of the 1995, 2001, and 2006 events, in gray (Delouis *et al.*, 1997; Bilek and Ruff, 2002; Delouis and Legrand, 2007). Black diamonds are the six strong-motion stations that recorded the 2007 mainshock diamonds: Iquique (IQUI), Pica (PICA), Tocopilla (TOCO), Calama (CALA), Mejillones (MEJI), and Antofagasta (ANTO). Dashed line: G1, seismic gap before the 2007 rupture and remaining gap for the occurrence of a very large ($M > 8.5$) event; G2, reduced gap, most likely place for the next large ($M > 7.5$) underthrusting event. (b) Cross section showing background seismicity from 1991 to 1994 well recorded by a local network between latitude 24.5° S and 22.5° S. Same longitude scale as in (a). The black line indicates the main slip zone during the 2007 Tocopilla event. The dashed line corresponds to the shallower part of the slip distribution in the southern part of the rupture (same horizontal and vertical scale).

seismic stations (short period and broadband) and compared to the slip distribution. A tight relation between the 2007 Tocopilla earthquake and the 1995 Antofagasta event is found, and the implication of the 2007 rupture for the northern Chile seismic gap is discussed.

Waveform Data

The Tocopilla earthquake was well recorded by the network of digital accelerometers installed in the region in 2001 (see the Data and Resources section). Strong-motion waveform modeling is performed on the displacement seismograms obtained from the acceleration records (Kinemetics Etna with episensors) after double integration in time and band-pass filtering. The six strong-motion stations incorporated in the analysis are situated at epicentral distances ranging from 26 to 235 km (Fig. 1). Absolute time, used in the process of locating the mainshock hypocenter, was provided by Global Positioning System (GPS) receivers.

Broadband seismograms of the mainshock recorded at teleseismic distances were obtained from the Incorporated Research Institutions for Seismology (IRIS) data center (see the Data and Resources section).

Data processing includes deconvolution from the instrument response, integration to obtain displacement, windowing around the *P*-(vertical) and *SH*-wave trains, equalization to a common magnification and epicentral distance, and band-pass filtering.

Mainshock Location

The mainshock was recorded by a small number of seismological stations at local distance. Five *P*- and *S*-wave arrival time pairs were obtained from the strong-motion records described previously, and one was obtained from broadband station LVC (Limon Verde, Deutsches GeoForschungsZentrum GEOPHON/GFZ, located 125 km to the east of the hypocenter). To determine how the hypocentral solution could be constrained with such limited data, we used a specific procedure combining a 1D systematic exploration with a global optimization scheme by simulated annealing. The search intervals, 25° S–21° S for latitude, 72° W–67° W for longitude, and 0 to 300 km for depth, are evenly sampled with a spacing of 2 km. Each parameter (latitude, longitude, and depth) is successively explored using the 1D sampling.

Each time a sampled value is tested, it is kept fixed in a simulated annealing inversion performed to find optimal values for the other two parameters. The criterion for selecting optimal solutions is the minimization of the root mean square (rms) error on arrival times. This procedure allowed us to map the rms error as a function of the parameter values. We obtained a single minimum of the rms error, corresponding to an epicenter located at 22.33° S, 70.16° W with an uncertainty of ±4 km, and a hypocentral depth of 45 ± 6 km.

Source depth was also confirmed by modeling the teleseismic waveforms.

The simulated annealing scheme used throughout this study, to locate the mainshock hypocenter and to invert for the slip distribution, was developed in previous studies (e.g., Delouis *et al.*, 2002) and is an adapted version of the algorithm presented in Corona *et al.* (1987) and Goffe *et al.* (1994).

Figure 1b displays background seismicity from 1991 to 1994 well located between latitude 24.5° S and 22.5° S by a local network (Delouis, 1996). Selected events have computed horizontal and vertical errors less than 5 km. The mainshock hypocenter is located within the shallow Wadati–Benioff zone.

The crustal model used throughout this study consists of five layers of thicknesses 5, 5, 10, 20, and 10 km and *P*-wave velocities 5.8, 6.1, 6.6, 7.1, and 7.5 km/sec, respectively, with a V_P/V_S ratio of 1.78. The mantle that follows is represented by a half-space with *P*-wave velocity 8.0 km/sec. This model is identical to the one used in the study of the 2003 Tarapaca event (Delouis and Legrand, 2007) except for the thickness of the lowermost crustal layer and for the V_P/V_S ratio.

Aftershocks

Three hundred eighty aftershocks occurring in the first two weeks (14 to 30 November 2007) following the mainshock were located using the local seismic stations displayed in Figure 2a. All stations were deployed in the few days following the mainshock by the Servicio Sismologico of the Universidad de Chile, except the northernmost one (PB01), which belongs to the GFZ Potsdam. A minimum of five *P* and one *S* arrival times have been used to locate hypocenters, using the Hypocenter code (Lienert and Havskov, 1995). The computed horizontal and vertical errors on the locations are 5.4 ± 2.3 km and 6.1 ± 3.0 km, respectively (average value plus or minus one standard deviation). Focal mechanisms of the largest aftershocks represented in Figure 2 are GCMT solutions. They are all similar to the mainshock mechanism, compatible with low-angle thrusting. The largest aftershock (M_w 6.8) occurred 24 hr after the mainshock. In cross section, aftershocks are concentrated along the plate interface, between 20 and 50 km depth. In addition, a reactivation of intermediate-depth seismicity occurred that was not observed in the months preceding the Tocopilla earthquake. These intermediate-depth events, not shown in this article, have normal faulting mechanisms, similar to that of the intermediate-depth earthquake of Tarapaca in 2005.

Fault Model and Waveform Inversion Procedure

First, we investigated the focal mechanism of the mainshock by modeling the *P* and *SH* broadband waveforms recorded at teleseismic distances with a double-couple point source, using the approach of Nabelek (1984). Then, the fault parameters were tested and adjusted with the slip inversion. Our best focal mechanism is (strike, dip, rake) = (0, 20, 105) where the rake is a slip-weighted average over the rupture area.

Kinematic modeling follows the approach of Delouis *et al.* (2002). The model consists of a single fault segment 192 km long and 132 km wide, subdivided into 176 subfaults measuring 12 km along strike and dip. Given the location of the event, the shallow nodal plane of the focal mechanism is expected to be the fault plane. The strike and dip angles of

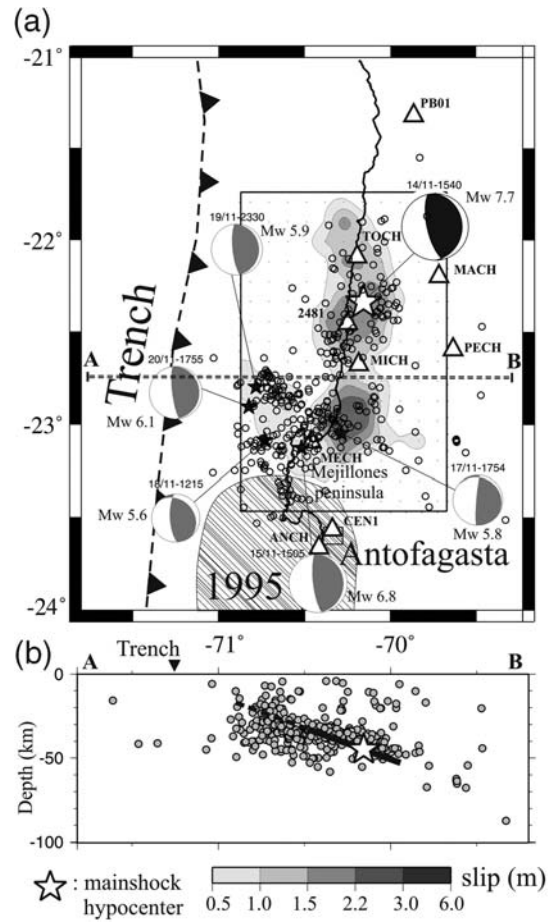

Figure 2. Close-up view showing the relation between the aftershocks and the slip distribution. Small circles are the aftershocks recorded and located by the local temporary seismic stations (triangles with names). The epicenters of the largest aftershocks are indicated by the black stars, all locally determined, associated with the GCMT solutions, best double-couple focal mechanism and M_w. Numbers above focal mechanisms are day/month-hour minute, all from 2007. The double dashed line AB indicates the cross-section line of (b). The focal mechanism of the mainshock is from this study. (b) Cross section displaying the aftershock and mainshock hypocenters. As in Figure 1, the black line indicates the main slip zone during the 2007 Tocopilla event. The dashed line corresponds to the shallower part of the slip distribution in the southern part of the rupture with the same horizontal and vertical scale. Only aftershocks with travel-time rms error < 0.3 sec are shown in (a) and (b) with the same longitude scale for (a) and (b).

the fault are kept fixed: (strike, dip) = (0°, 20°). Rupture initiation in the model coincides with the geographic hypocenter (22.33° S, 70.16° W, 45 km depth). The continuous rupture is approximated by a summation of point sources evenly distributed on the fault plane: one at the center of each subfault. A nonlinear inversion is performed with simulated annealing. For each point source, a local source time function is defined, corresponding to the rate of seismic moment locally released, represented by two mutually overlapping isosceles triangular functions of 1.5 sec duration each. For each of the 176 subfaults (points sources), the parameters to be inverted for are the slip onset time, the rake angle, and the amplitudes of the two triangular functions. The simulated annealing scheme requires the definition of bounding values for each of the free parameters. Subfault slip onset times are allowed to vary within the interval defined by two limiting rupture velocities, 1.5 and 3.2 km/sec. The rake angle may vary between 90° and 120°. The amplitudes of the triangular functions are limited so that the total slip on a subfault may vary between 0 and 6 m. Convergence of the simulated annealing procedure is based in this study on the simultaneous minimization of the rms waveform misfit and of the total seismic moment. The rms misfit error is the average of the normalized rms errors of the individual datasets (teleseismic and strong motion), equally weighted here. Minimization of the total seismic moment is required to reduce spurious slip in the fault model.

Synthetic seismograms at strong-motion stations are computed using the discrete wavenumber method of Bouchon (1981). Synthetic seismograms at teleseismic stations were generated using ray-theory approximation and the approach by Nabelek (1984).

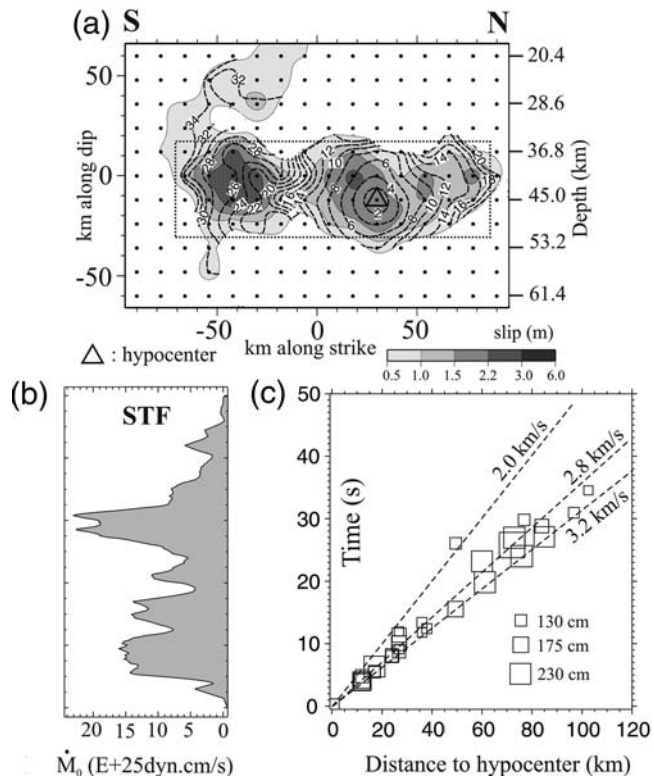

Figure 3. Rupture model resulting from the joint inversion of teleseismic and strong-motion data. (a) Slip map and rupture onset time isochrones (dashed lines with labels in seconds). Slip less than 0.5 m is not represented. The dotted rectangular frame delineates the main slip zone. The grid of black dots corresponds to the location of the point sources used to simulate the continuous rupture. (b) Moment rate source time function (STF) for the whole rupture. (c) Rupture timing. Each open square represents the slip of an individual subfault with a size proportional to slip. Dashed lines corresponding to constant rupture velocities 2.0, 2.8, and 3.2 km/sec are drawn for reference. Slip less than 1 m is not represented. (b) and (c) have the same vertical time scale.

Inversion Results

From the hypocenter located near the downdip end of the assumed coupled zone, the rupture propagated laterally, expanding 50 km to the north and 100 km to the south. Most of the slip occurred south of the hypocenter and in the depth range 35–50 km (Fig. 3a) in two slip patches. The first slip patch comprises the hypocenter. The second slip patch is located 70 km more to the south. There, slip reached 3 m. Some slip occurred at shallower depth in the south, with an amplitude essentially below 1 m. We outlined the main slip zone containing the two patches in Figure 3a (dotted rectangle), where the average slip is 1.2 m for an area of 156×48 km^2.

Overall, the waveforms are correctly modeled in amplitude and phase (Figs. 4 and 5), indicating that the rupture model is adequate, with no need for additional fault complexity. A notable exception is the east component of strong-motion station ANTO, whose amplitudes could not be matched. The rupture propagated at an average velocity of 2.8 km/sec, without large variations (Fig. 3c). Total source duration is 45 sec, but most slip occurred within the first 35 sec after origin time (Fig. 3b). The total seismic moment is 4.5×10^{20} N m, corresponding to M_w 7.7.

Synthetic tests were carried out in order to assess how the resolution of the slip distribution may vary on the fault model when inverting separately and jointly the teleseismic and strong-motion datasets (Fig. 6). A synthetic fault model comprising six slip patches rupturing at a constant velocity (2.7 km/sec) was used to generate synthetic data at the teleseismic and strong-motion stations. In each patch, slip is constant and equal to 2.7 m (Fig. 6a). The synthetic data so generated were inverted using the same inversion scheme and parameters as for the real data case. Slip from the teleseismic inversion (Fig. 6b) tends to be too smooth in the upper and lower parts of the fault model. The strong-motion inversion (Fig. 6c) better locates the individual slip patches, and the joint inversion (Fig. 6d) provides the most accurate image of the slip distribution, with the six slip patches recovered and separated by nonslipping areas. This test indicates that the position and approximate shape of the main slip

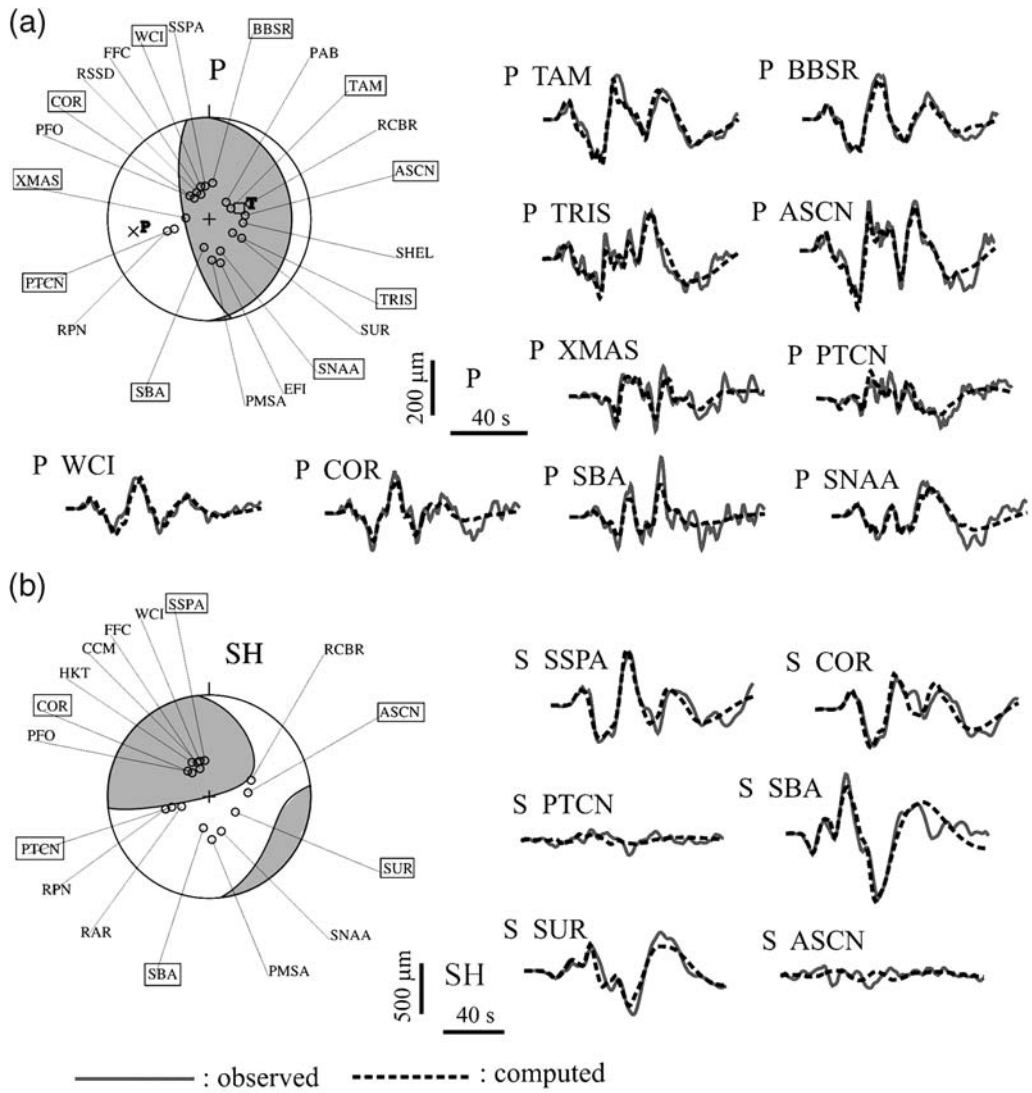

Figure 4. Modeling of the (a) *P* and (b) *SH* teleseismic waveforms from the joint inversion. The *P* and *SH* focal mechanisms are shown with the station distribution. Only waveforms at stations whose name is framed are drawn. Normalized waveform misfit rms is 0.42.

patches resulting from the joint inversion can be trusted but probably not the details inside individual patches. The maximum slip found by the joint inversion for patches 1–6 is 2.8, 2.6, 3.4, 2.8, 3.4, and 2.0 m, respectively, to be compared to the 2.7 m of the synthetic model. The slip averaged rupture velocity found by the teleseismic, strong-motion, and joint inversions are 2.59, 2.61, and 2.63 km/sec, respectively, to be compared to the 2.7 km/sec of the synthetic model, remembering that in the inversion rupture velocity is allowed to vary between 1.5 and 3.2 km/sec.

The separate and joint inversions of the real data can be compared in Figure 7. The two datasets, teleseismic and strong motion, provide similar results, with a slip distribution dominated by two slip patches. However, the definition of the patches is sharper in the strong-motion case. The normalized rms errors of the data fit and seismic moment resulting from the different inversions are given in Table 1. The rms data fit errors from the joint inversion are only slightly larger than those resulting from the separate inversions, meaning that there is no significant incompatibility between the two datasets. We note however, that the teleseismic data can be matched with a seismic moment 20% smaller than the strong-motion data (Table 1).

We tested the second nodal plane of the focal mechanism, $(\text{strike}, \text{dip}, \text{rake}) = (165, 71, 85)$, corresponding to a steep west dipping fault plane. The data fit in the joint inversion is clearly degraded with respect to the shallow east dipping fault model (Table 1), confirming the fault choice.

Discussion and Conclusion

A detailed description of the rupture process of the M_w 7.7 Tocopilla earthquake could be obtained from the combined analysis of the strong-motion and teleseismic records: location of rupture initiation, focal mechanism, and slip distribution. Slip occurred at the base of the coupled

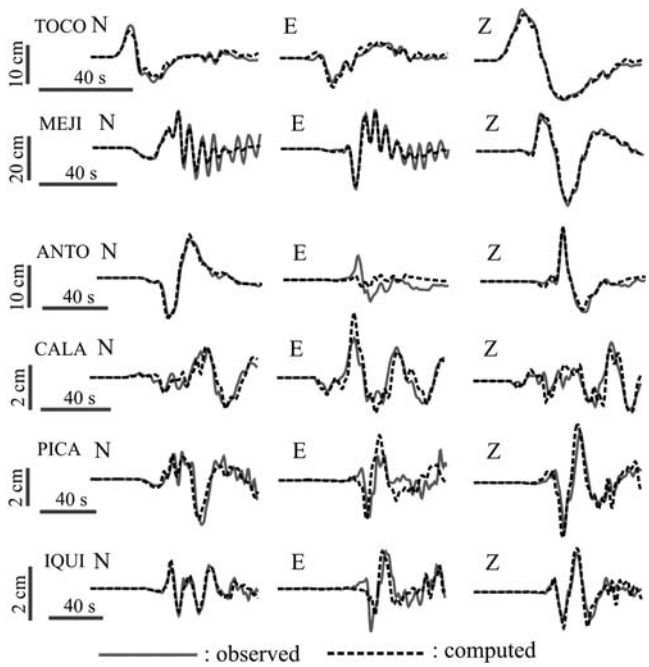

Figure 5. Modeling of the strong-motion waveforms from the joint inversion. Seismograms are in displacement, filtered between 0.01 and 0.03 Hz, depending on the station, and 0.25 Hz. Normalized waveform misfit rms is 0.23.

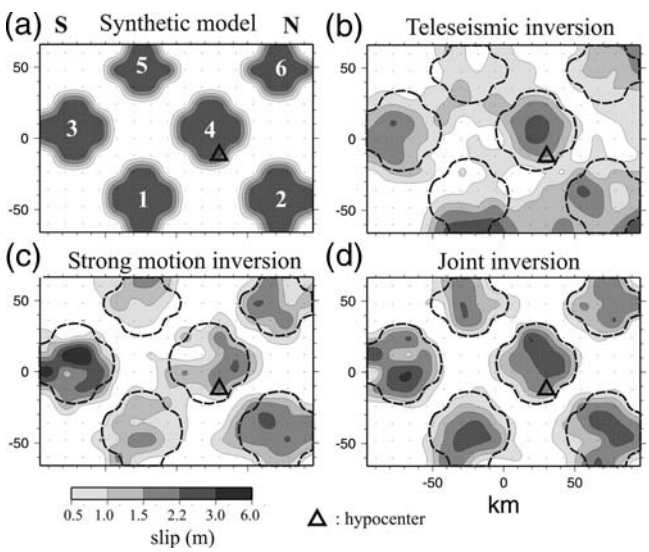

Figure 6. Resolution test. A synthetic model was defined to compute synthetic signals that were inverted using the same approach as for the real data. The synthetic model, with six slip patches numbered with white figures is shown in (a), and the slip maps corresponding to the teleseismic, strong-motion, and joint inversion are displayed in (b), (c), and (d), respectively. In the inversion maps (b), (c), and (d), the dashed lines indicate the contours of the slip patches from the synthetic model (a). Note the improvement of resolution with the joint inversion (d).

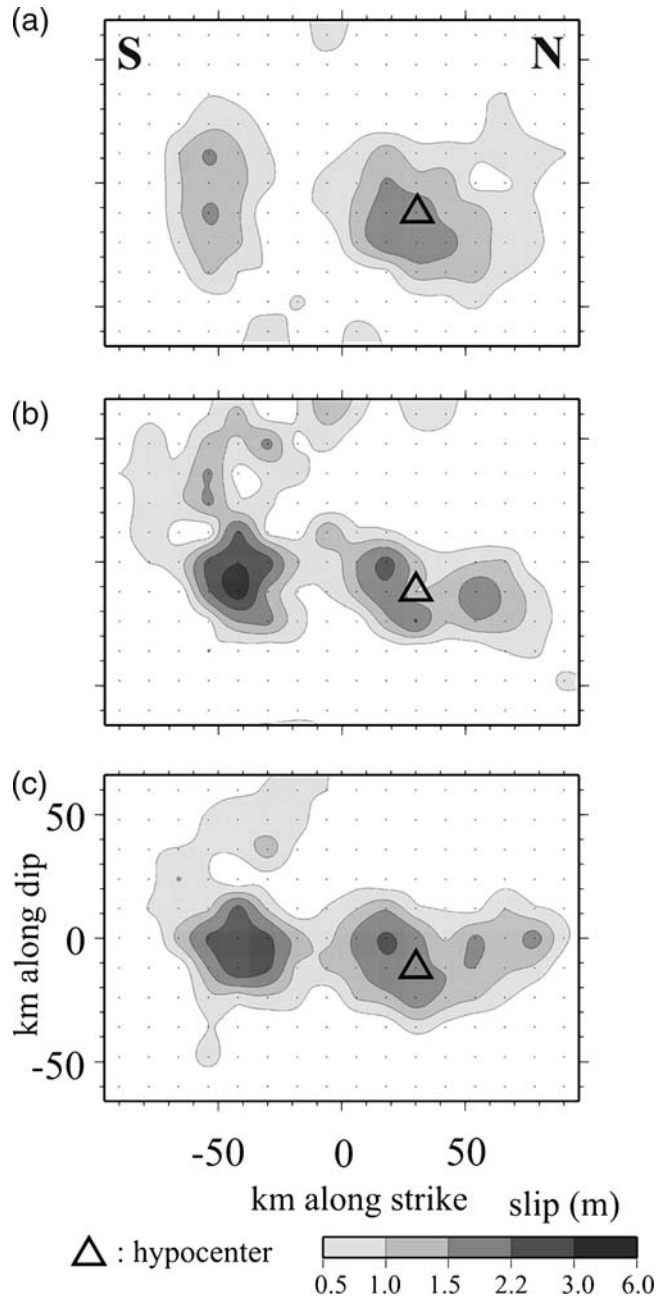

Figure 7. Comparison of the slip distributions obtained from the inversions of (a) teleseismic, (b) strong-motion, and (c) joint datasets.

zone of the plate interface, with little fault motion above 35 km depth. These characteristics explain the much reduced size of the tsunami which was produced.

The southernmost part of the November 2007 rupture connects precisely with the northern termination of the 1995 Antofagasta rupture (Figs. 1 and 2). We observe that the main slip patch of the 2007 rupture is separated from the end of the 1995 rupture zone by an area 20 km wide characterized by moderate slip less than 1 m. This border zone between the 1995 and 2007 ruptures is located below the northern part of

Table 1

Normalized rms Error of the Data Fit and Seismic Moment (M_0) for the Different Inversions Carried Out

	Low-Angle East Dipping Fault Model			Steep West Dipping Fault Model		
	rms Teleseismic data	rms Strong-Motion data	M_0 (N.m)	rms Teleseismic data	rms Strong-Motion data	M_0(N m)
Teleseismic data inversion	0.42		3.97×10^{20}			
Strong-motion data inversion		0.23	4.76×10^{20}			
Teleseismic and strong-motion data inversion	0.46	0.29	4.50×10^{20}	0.53	0.49	4.40×10^{20}

Results of the separate and joint inversions are given for the low-angle east dipping fault plane, which is assumed to be the rupture plane. For the fault plane steeply dipping to the west, only the joint inversion has been performed.

the Mejillones peninsula. This area was already proposed to have acted as a barrier for the 1995 rupture, interrupting the propagation of this event towards the north (Delouis *et al.*, 1997). The barrier role of the Mejillones peninsula appears to be confirmed by the termination of the 2007 rupture. Pritchard and Simmons (2006) proposed that the plate interface below the Mejillones peninsula may be decoupled, as suggested by the occurrence there of large afterslip following the 1995 Antofagasta earthquake. If it is the case, the peninsula would act as a damping barrier for seismic ruptures. The possibility for a larger event ($M_w > 8.5$) to break through the entire Mejillones peninsula cannot be excluded however.

We observe a good agreement between the downdip end of the 2007 rupture and the downdip limit of the dense aftershock zone, at 50 km depth (Fig. 2b). A similar relationship had been observed for the 1995 Antofagasta earthquake (Delouis *et al.*, 1997). It strongly suggests that the downdip end of the seismically coupled zone is located at 50 km depth, as indicated as well by the change from underthrusting to normal faulting mechanisms (Comte and Suárez, 1995; Delouis *et al.*, 1996). We observe also a strong correlation between the slip distribution and the aftershocks in map view (Fig. 2a). In detail, aftershocks tend to be more densely concentrated at the edge of high slip areas, as well as within the slip zone rising trenchward near the northern tip of the Mejillones peninsula (Fig. 2a).

The M_w 7.7 Tocopilla earthquake of November 2007 contributed only weakly to the rupturing of the seismic gap of northern Chile. If 100% of seismic coupling is assumed, the total slip deficit reaches more than 10 m since 1877. The 1.2 m of average and 3 m of peak slip associated with the 2007 earthquake would represent only a small fraction of the total amount of accumulated slip deficit. On the other hand, as proposed by Chlieh *et al.* (2004), the lower part of the seismically coupled interface may behave as a transition zone between a fully locked (shallower) and a stable (deeper) plate interface, accommodating both aseismic and seismic slip through time. In that case, slip deficit and stress would now be more concentrated in the shallowest part of the plate interface, updip of the 2007 rupture.

The dimension of the seismic gap of northern Chile after the 2007 event may be measured in two ways: the 400 km long segment from Tocopilla to Ilo (G2 in Fig. 1a) may be considered as the most likely place for the next large ($M > 7.5$) underthrusting event at the base of the coupled zone. However, the 550 km long segment from Antofagasta to Ilo (G1 in Fig. 1a) is most certainly still a gap for a very large ($M > 8.5$) subduction earthquake. In the most favorable (less disastrous) case, where the smallest maximum segment available for rupture is considered (G2, 400 km long), the 2007 Tocopilla event may nonetheless announce a much larger earthquake.

Data and Resources

Focal mechanisms from the Global Centroid Moment Tensor (GCMT) catalog were obtained from www.globalcmt.org/CMTsearch.html (last accessed January 2008). Strong-motion data were obtained from the joint accelerometric network of the Geophysics and Civil Engineering departments of the University of Chile (www.cec.uchile.cl/~ragic/ragic.htm, last accessed November 2007). Broadband seismological records were obtained from the Incorporated Research Institutions for Seismology (IRIS) Data Management Center, using the WILBER II search (www.iris.edu/cgi-bin/wilberII_page1.pl, last accessed November 2007). Some figures were partly made using Generic Mapping Tools (GMT) package by Wessel and Smith (www.soest.hawaii.edu/gmt, last accessed January 2008). Seismic data processing was partly done using the Seismic Analysis Code (SAC) package by Peter Goldstein (http://www.iris.edu/software/sac/sac.request.htm, last accessed September 2008).

Acknowledgments

We thank the Servicio Sismologico of the Universidad de Chile for providing the aftershocks seismograms. We are grateful to the Departamento de Ingeniería Civil de la Universidad de Chile, and in particular, Pedro Soto, for maintaining the accelerometric network and providing an easy access to the strong-motion data. The manuscript was improved thanks to the help of two anonymous reviewers. This work was partially funded by the European Community SAFER (Seismic eArly warning For EuRope) project.

References

Bilek, S. L., and L. J. Ruff (2002). Analysis of the 23 June 2001 $M_w = 8.4$ Peru underthrusting earthquake and its aftershocks, *Geophys. Res. Lett.* **29,** no. 20, 21.1–21.4, doi 10.1029/2002GL015543.

Bouchon, M. (1981). A simple method to calculate Green's functions for elastic layered media, *Bull. Seismol. Soc. Am.* **71,** no. 4, 959–971.

Chlieh, M., J. B. de Chabalier, J. C. Ruegg, R. Armijo, R. Dmowska, J. Campos, and K. L. Feigl (2004). Crustal deformation and fault slip during the seismic cycle in the north Chile subduction zone, from GPS and InSAR observations, *Geophys. J. Int.* **158,** 695–711.

Comte, D., and M. Pardo (1991). Reappraisal of great historical earthquakes in the northern Chile and southern Peru seismic gaps, *Nat. Hazards* **4,** 23–44.

Comte, D., and G. Suárez (1995). Stress distribution and geometry of the subducting Nazca plate in northern Chile using teleseismically recorded earthquakes, *Geophys. J. Int.* **122,** 419–440.

Corona, A., M. Marchesi, C. Martini, and S. Ridella (1987). Minimizing multimodal functions of continuous variables with the 'simulated annealing' algorithm, *ACM Trans. Math. Softw.* **13,** 262–280.

Delouis, B. (1996). Subduction et déformation continentale au Nord-Chili, *Ph.D. Thesis*, Université Louis Pasteur de Strasbourg, France, 262 pp.

Delouis, B., A. Cisternas, L. Dorbath, L. Rivera, and E. Kausel (1996). The Andean subduction zone between 22 and 25S (northern Chile): precise geometry and state of stress, *Tectonophysics* **259,** 81–100.

Delouis, B., and D. Legrand (2007). The M_w 7.8 Tarapaca intermediate depth earthquake of 13 June 2005 (northern Chile): fault plane identification and slip distribution by waveform inversion, *Geophys. Res. Lett.* **34,** L01304, doi 10.1029/2006GL028193.

Delouis, B., D. Giardini, P. Lundgren, and J. Salichon (2002). Joint inversion of InSAR, GPS, teleseismic and strong motion data for the spatial and temporal distribution of earthquake slip: application to the 1999 Izmit mainshock, *Bull. Seismol. Soc. Am.* **92,** 278–299.

Delouis, B., T. Monfret, L. Dorbath, M. Pardo, L. Rivera, D. Comte, H. Haessler, J. P. Caminade, L. Ponce, E. Kausel, and A. Cisternas (1997). The $M_w = 8.0$ Antofagasta (Northern Chile) earthquake of 30 July, 1995: a precursor to the end of the large 1877 gap, *Bull. Seismol. Soc. Am.* **87,** 427–445.

Goffe, W. L., G. D. Ferrier, and J. Rogers (1994). Global optimization of statistical functions with simulated annealing, *J. Econ.* **60,** no. 1/2, 65–99.

Lienert, B. R. E., and J. Havskov (1995). A computer program for locating earthquakes both locally and globally, *Seism. Res. Lett.* **66,** 26–36.

Nabelek, J. (1984). Determination of earthquake fault parameters from inversion of body waves, *Ph.D. Thesis*, Massachusetts. Institute of Technology, Cambridge, Massachusetts, 361 pp.

Pritchard, M. E., and M. Simons (2006). An aseismic slip pulse in northern Chile and along-strike variations in seismogenic behavior, *J. Geophys. Res.* **111,** B08405, doi 10.1029/2006JB004258.

Pritchard, M. E., C. Ji, and M. Simons (2006). Distribution of slip from 11 $M_w > 6$ earthquakes in the northern Chile subduction zone, *J. Geophys. Res.* **111,** B10302, doi 10.1029/2005JB004013.

Ruegg, J. C., J. Campos, R. Armijo, S. Barrientos, P. Briole, R. Thiele, M. Arancibia, J. Cañuta, T. Duquesnoy, M. Chang, D. Lazo, H. Lyon-Caen, L. Ortlieb, J. C. Rossignol, and L. Serrurier (1996). The $M_w =$ 8.1 Antofagasta (north Chile) earthquake of July 30, 1995: first results from teleseismic and geodetic data, *Geophys. Res. Lett.* **23,** 917–920

U.S. Geological Survey (2007a). Historic earthquake web page, http://earthquake.usgs.gov/eqcenter/eqinthenews/2007/us2007jsat/#summary (last accessed January 2008).

U.S. Geological Survey (2007b). M7.7 northern Chile, earthquake of 14 November 2007, ftp://hazards.cr.usgs.gov/maps/sigeqs/20071114/20071114.pdf (last accessed January 2008).

Vallée, M. (2007). $M_w = 7.6$ Chile-Antofagasta earthquake, http://www-geoazur.unice.fr/SEISME/CHILI141107/note1.html (last accessed January 2008).

Géosciences Azur
University of Nice
Sophia Antipolis, CNRS, IRD
250 rue A. Einstein
Valbonne, 06560, France
delouis@geoazur.unice.fr
monfret@geoazur.unice.fr
(B.D., T.M.)

Departamento de Geofisica
Universidad de Chile
Blanco Encalada 2002
Santiago, Chile
mpardo@dgf.uchile.cl
denis@dgf.uchile.cl
(M.P., D.L.)

Manuscript received 13 February 2008